Rotor loads prediction on UH-60A flight test using loose fluid/structure coupling

Rocco Moretti, Hyeonsoo Yeo, Francois Richez, Biel Ortun

Rotor Loads Prediction on UH-60A Flight Test using Loose Fluid/Structure Coupling

Rocco Moretti
Research Scientist
ONERA, the French Aerospace Lab
Meudon, France

Hyeonsoo Yeo
Research Aerospace Engineer
U.S. Army Combat Capabilities Development Command
Aviation & Missile Center
Ames Research Center, Moffett Field, CA, USA

François Richez **Biel Ortun**
Research Scientists
ONERA, the French Aerospace Lab
Meudon, France

ABSTRACT

This work exploits the high-quality UH-60A flight test campaign for comparison with concurrent simulations at the U.S. Army and ONERA. Rotor airloads and structural loads are predicted by coupling Computational Fluid Dynamics (CFD) with rotorcraft comprehensive analysis (CA). A high-speed test point is examined. Comparisons are shown for airloads, structural loads and rotor controls. Agreement with test data is improved when the flexibility of the pitch link is considered. Results show good agreement between the two partners predictions and with test data.

INTRODUCTION

In the last decades, numerical simulation has taken its place in the study of aerodynamic loads on aircraft and helicopters. It is essential to reveal and resolve possible design deficiencies/inconsistencies before wind tunnel or flight tests are performed.

In the case of helicopters, accurate rotor loads prediction is a really challenging task because of the interaction of several complex phenomena: unsteady low-speed and transonic aerodynamics of flexible blades undergoing large displacements and rotations. This work validates rotor loads prediction with existing tools at ONERA and U.S. Army on the UH-60A flight test data (Ref. 1). Similar comparison has already been carried out on ONERA 7A rotor (Refs. 2, 3). The UH-60A rotor has already been extensively studied by the U.S. Army (Refs. 4,5).

The state-of-the-art in the rotor loads prediction is coupling the rotorcraft comprehensive analysis (CA) with the computational fluid dynamics (CFD) (Ref. 5). Indeed, this allows to improve fidelity of aerodynamics by replacing the CA low-order aerodynamic model with the most accurate flow solver for this kind of computations.

The novelty of this work stands on four points: (1) The cooperation between the U.S. Army Combat Capabilities Development Command Aviation & Missile Center (DEVCOM AvMC) and the ONERA French Aerospace Research Lab for the analysis of the UH-60A rotor under the United States/France Project Agreement on Rotary-Wing Aeromechanics and Human Factors Integration Research, (2) Success of ONERA's coupled CFD/CA methodology on the prediction of the UH-60A rotor loads, (3) Systematic comparison of two high-fidelity CFD/CA coupled analyses, and (4) Demonstration of how simple assumptions on blade modeling in the CA tool can have an important impact on rotor loads prediction.

The test data used in the present study were obtained during the NASA/Army UH-60A Airloads Program conducted from August 1993 to February 1994 (Figure 1). This seminal flight-test program provided a detailed airloads and blade structural loads database for a full-scale rotor covering a broad flight envelope. The UH-60A main rotor is a four-bladed, articulated rotor. The blade construction uses a titanium spar with a fiberglass outer contour and two airfoils, the SC1095 and SC1094R8 (Figure 2).

The present study investigates a high-speed flight condition: counter c8534, $\mu = 0.37$, $C_T/\sigma = 0.081$, with advancing blade negative lift.

COMPUTATIONAL METHODOLOGIES

Rotor loads prediction is accomplished by coupling a rotor comprehensive analysis with a CFD code solving the Unsteady Reynolds-averaged NavierStokes equations (URANS). The CFD airloads replace, through a delta method, the air-

Presented at the Vertical Flight Society's 79th Annual Forum & Technology Display, West Palm Beach, FL, USA, May 16–18, 2023.

Figure 1. UH-60A flight test picture.

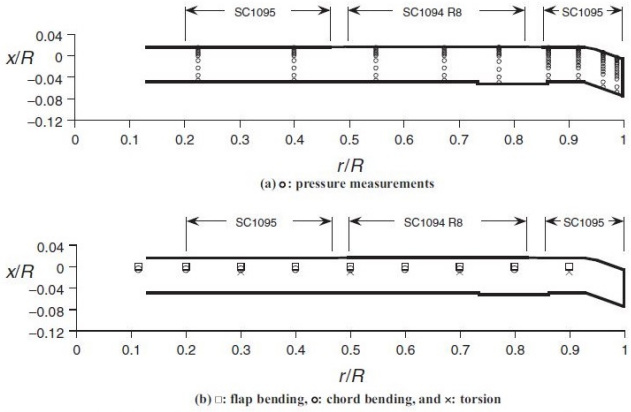

Figure 2. UH-60A rotor blade planforms showing locations of airfoil section, pressure taps and strain gauges.

loads of the CA. The coupling exchanges are done on a per revolution (periodic) basis (loose coupling).

U.S. Army used RCAS (Ref. 6) for comprehensive analysis and Helios (Ref. 7) for CFD. RCAS is a comprehensive multidisciplinary computer software system for predicting rotorcraft aerodynamics, performance, stability and control, aeroelastic stability, loads, and vibration. RCAS is capable of modeling a wide range of complex rotorcraft configurations operating in hover, forward flight, and maneuvering conditions. RCAS has been used extensively for correlation of performance and loads measurements of the UH-60A in various flight conditions. Helios is the rotary-wing product of the U.S. Army and CREATE Air Vehicles program sponsored by the U.S. Department of Defense High Performance Computing Modernization Office. Helios uses an innovative dual-mesh paradigm that employs unstructured meshes in the near body close to the surface to capture the wall-bounded viscous effects and structured Cartesian grids in the off body to resolve the wake through a combination of higher-order algorithms and adaptive mesh refinement (AMR). The unstructured solver NSU3D is used for near-body and the structured solver SAMARC is used for the Cartesian off-body grid system. An overset procedure facilitates the data exchange and also enables the relative motion between the two meshes. The parallel domain connectivity solver PUNDIT automatically handles the data exchange between the two meshes.

ONERA used HOST (Ref. 8) for comprehensive analysis and

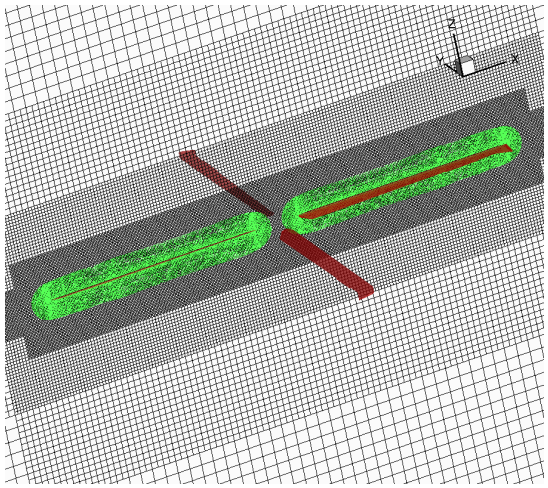

Figure 3. Structured overset grids.

elsA (Ref. 9) for CFD. HOST (Helicopter Overall Simulation Tool) is a rotorcraft comprehensive analysis developed by Airbus Helicopters. HOST modeling of blade dynamics is multibodylike. The blade is represented by a series of rigid elements connected by virtual hinges. Inertial properties (e.g., mass and moment of inertia) are assigned to each rigid element, and elastic properties (e.g., flap bending, chord bending, and torsion stiffness) are assigned to each hinge. A modal reduction approach is used to reduce the number of degrees of freedom from a large system of equations. The aerodynamics of HOST is based on a lifting-line approach based on airfoil tables combined with a wake model. In this effort, among the several wake models available, a prescribed wake helical geometry was used. The elsA CFD code, developed at ONERA, solves the unsteady Reynolds-averaged Navier Stokes equations for both background Cartesian grids and blade curvilinear grids. An overset procedure facilitates the data exchange and also enables the relative motion between the two meshes. The near-body grids of the blades are rotated and deformed following the blade motion and trim provided, through the loose coupling, by the rotorcraft comprehensive analysis HOST.

In the current work, ONERA and U.S. Army used similar grid meshes. Helios used unstructured near-body grids, whereas elsA used structured near-body grids, see Figure 3. The four rotor blade grids in Helios have 15.4 million nodes and 36.5 million cells, whereas in elsA the cell count is 16 million. The finest off-body spacing in Helios is 5% chord with a fixed refinement region surrounding the rotor plane. The off-body grid contains 146 million unblanked grid points on 8 levels. In elsA, the finest off-body spacing is 10% chord.

Table 1 summarizes the main parameters characterizing the rotor and the studied flight point.

RESULTS

The results chapter is organised in two parts: the first part shows how the structural modeling of the UH-60A blade in HOST was modified in order to model the pitch link stiffness

Table 1. Summary of UH-60A rotor flight test

Characteristic	Symbol	Value
Rotor Geometry		
Rotor radius	R	26.833 ft (8.179 m)
Mean blade chord	c	1.722 ft (0.525 m)
Number of blades	N_b	4
Rotor solidity	σ	0.0817
Airfoils		SC1095,SC1094R8
UH-60A test point C8534: High speed		
Air density	ρ_{inf}	0.002082 $slug/ft^3$
Air density (metric)	ρ_{inf}	1.0732 kg/m^3
Air temperature	T_{inf}	71.8 F (295.3 K)
Rotational speed	Ω	258.1 rev/min
Advance Ratio	μ	0.37
Rotor thrust coefficient	C_T/σ	0.081
Sideslip angle	β	1.27 deg

and hence become comparable to RCAS. This was achieved by modifying the inboard torsional stiffness in HOST and comparing the Campbell diagrams produced by HOST and RCAS.

Once the structural models are shown to be equivalent, the second part compares the airloads, structural loads and control angles.

Campbell diagrams

Structural dynamics modeling of the UH-60A rotor blade is briefly described. Figure 4 shows the RCAS modeling of the rotor hub with blade hinges, pitch control, and the lag damper. The blade is composed of 13 nonlinear beam elements. Three coincident hinge elements are offset from the center of rotation. The three hinge elements allow for simultaneous flap, lag, and pitch rotations of the blade. Rigid bars and spring elements are used to represent the pitch control linkage.

HOST assumes, by default, the pitch link to be rigid (i.e., infinite stiffness). An equivalent pitch link model was developed in this work by using torsionally soft beam element. More recently a pitch control elasticity model has been introduced in HOST by its main developers at Airbus Helicopters, but the authors did not have the time to use it for this paper. Detailed blade frequency comparisons are shown below. Campbell diagrams are calculated in vacuum conditions.

First are compared the Campbell diagrams when considering a rigid pitch link in HOST and the nominal pitch link stiffness in RCAS, see Figure 5. It can be seen that there is a good agreement for the lower modes, while significant differences arise in the torsion mode.

The flexibility of the pitch link is then introduced in HOST by lowering the torsional stiffness of the blade at the radius corresponding to the attachment of the pitch link. This process was done iteratively, judging by the agreement between RCAS and HOST. Eventually, a torsional stiffness adjustment

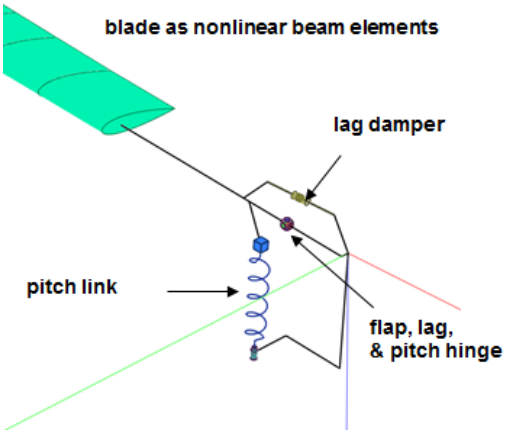

Figure 4. RCAS modeling of the UH-60A rotor.

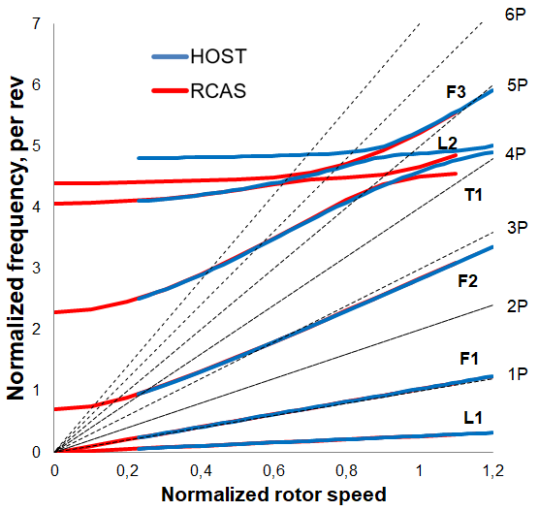

Figure 5. Fan plot; rigid pitch link in HOST.

was obtained such that an equivalent pitch link behaviour was created in HOST, yielding a very good agreement with the RCAS Campbell diagram, see Figure 6.

As a conclusion, this chapter has shown the relevance of modeling properly the pitch link stiffness in the rotorcraft comprehensive analyses. The remainder of the results presented in this paper correspond to coupled CFD/CA analyses and include this modeling.

Airloads

In this work calculated airloads were obtained by integrating pressure all over the chord, and not only at the location of the pressure taps. This is expected to be acceptable given that up to 30 unsteady pressure transducers were installed at every instrumented section of the UH-60A blade (Ref. 10), yet any error in the blade pressures may change significantly the integrated pitching moments. Consequently, all plots of pitching moment have the mean removed.

Figures 7 and 8 compare the normal force and pitching moment, respectively, at three span-stations. The black line corresponds to measurement. Blue, to Helios/RCAS calcula-

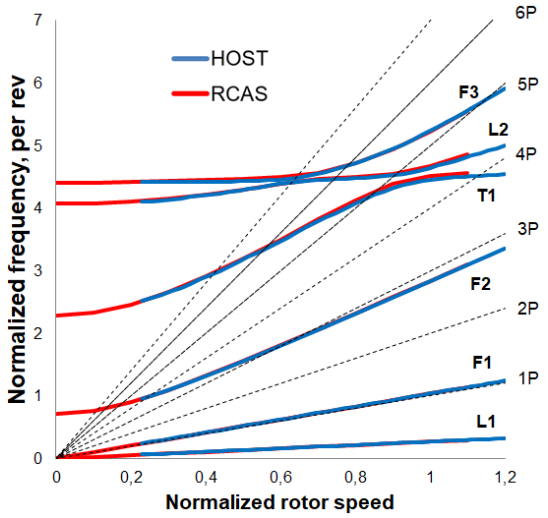

Figure 6. Fan plot; equivalent pitch link model in HOST.

tions. And then elsA/HOST calculations come in two types: dashed red line corresponds to elsA/HOST with rigid pitch link. Solid red line is the elsA/HOST calculation meant to be equivalent to Helios/RCAS, where pitch link flexibility is modelled. Normal force is characterized by a peak of negative lift at the tip of the advancing blade, and both Helios/RCAS and elsA/HOST capture this negative lift. The elsA/HOST with equivalent pitch link features a better agreement with Helios/RCAS than elsA/HOST with rigid pitch link. Elastic pitch link improves match with experiment on the retreating side, though in the first quarter, especially at r/R=0.865 and r/R=0.965, the rigid pitch link provides better agreement with test data.

Pitching moment is marked by a pronnounced negative, nose-down, pitching moment on the advancing side, resulting from the highly compressible flow on the outboard part of the blade. Agreement between both partners calculations and test data is good, although less so for the most outboard section, at r/R=0.965.

Trim control angles

The rotor control angles used for trimming the simulation are the collective pitch angle, the lateral cyclic pitch angle and the longitudinal cyclic pitch angle. Rotor shaft angle of attack is prescribed at the experiment value, -7.31 deg. Table 2 compares the experiment control angles and the predicted control angles at the convergence of the loose coupling. Agreement is best for the collective pitch angle. The largest differences are found in the longitudinal cyclic pitch angle, where the U.S. Army predicts an angle nearly 2 degrees smaller (in absolute value) than measurement, while ONERA underestimation is close to 3 degrees. Previously published work by the U.S. Army (Ref. 4) showed Helios/CAMRAD II to calculate very similar pitch control angles compared to Helios/RCAS for point c8534.

Table 2. UH-60A c8534 control angles

	Collective θ_0	Lateral cyclic θ_{1c}	Long. cyclic θ_{1s}
c8534	13.73	2.84	-11.05
Helios/RCAS	13.61	1.81	-9.35
elsA/HOST	13.87	3.38	-8.23

Structural loads

Figure 9 compares the calculated and measured oscillatory flap bending moment at r/R=0.113, 0.30, 0.50 and 0.70. The two coupled anlayses (elsA/HOST and Helios/RCAS) agree well with each other and with experiment. The equivalent pitch link model reduces amplitude at r/R=0.7 compared to the rigid pitch link model, and thus improves the correlation with test data. Figure 12 compares the half peak-to-peak flap bending moment. The rigid pitch link model significantly overpredicts the half peak-to-peak amplitude at the outboard locations. The equivalent pitch link model improves the correlation by decreasing the half peak-to-peak amplitude. Due to strong couplings among the high-frequency modes shown in Figure 6, pitch link stiffness has an important influence on flap bending moment. Overall, elsA/HOST tends to overpredict the amplitudes between r/R=0.40 and r/R=0.70, while the opposite is true for Helios/RCAS.

Figure 10 compares the calculated and measured oscillatory chord bending moment at r/R=0.113, 0.30, 0.50 and 0.70. Here the differences between the two coupled anlayses (elsA/HOST and Helios/RCAS) are more marked than for the flap bending moment, although both capture the experimental trends. Figure 13 compares the half peak-to-peak chord bending moment, showing for elsA/HOST a closer match to experiment. The significant underprediction of half peak-to-peak chord bending moment was previously observed by both RCAS and CAMRAD II (Ref. 4).

Figure 11 compares the calculated and measured oscillatory torsion moment at r/R=0.30 and 0.70. Modelling a rigid or flexible pitch link in HOST has a visible influence on the predicted torsion moment, with the rigid pitch link exhibiting higher amplitude oscillations and fewer harmonic content. Figure 14 compares the half peak-to-peak torsion moment and shows that the equivalent pitch link model substantially improves the correlation with the test data and both partners underestimate the torsion moment amplitude in the outboard part of the blade.

Finally, Figure 15 compares the harmonic magnitude of calculated and measured structural loads. In this comparison, elsA/HOST analysis results with rigid pitch link are not included for clarity. This comparison is analysed next in the light of the following assumptions: harmonics 1 and 2 are more related to rotor trim, lag damper and pitch-lag coupling. Harmonics higher than 2 are dominated by the blade elastic model and the coupling with the drivetrain. On the two first harmonics, the U.S. Army calculations (Helios/RCAS) feature better agreement with experiment, particularly for flap bending moment and torsion moment. The two first

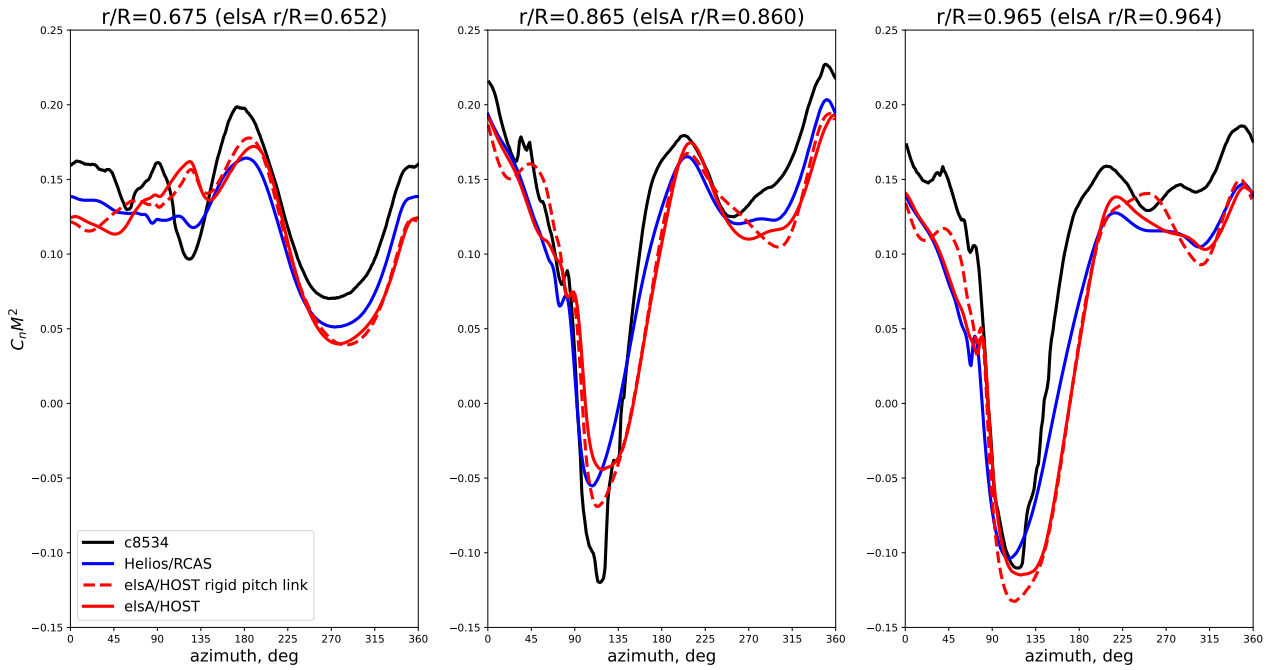

Figure 7. Sectional normal force coefficient C_nM^2.

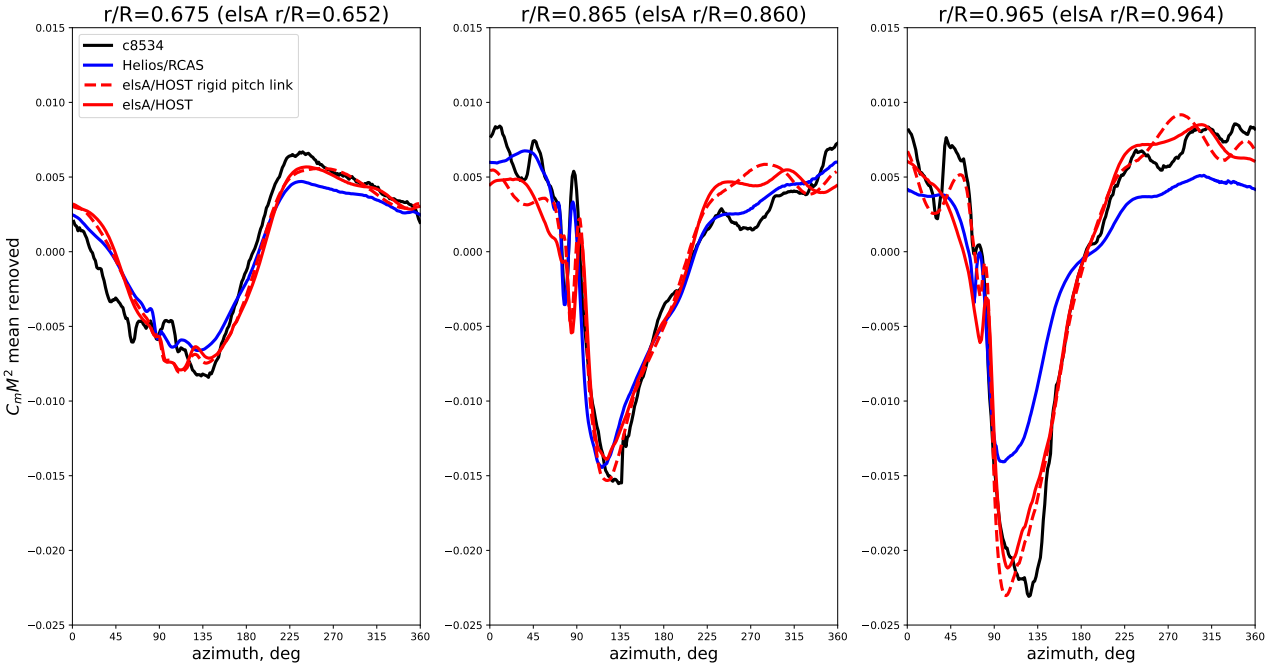

Figure 8. Sectional pitching moment coefficient C_mM^2 (mean removed).

harmonics of chord bending moment are harder to capture; elsA/HOST shows a quadratic trend, whereas Helios/RCAS a more linear one. Measurements are somewhere in-between. However, the elsA/HOST worsening agreement with experiment at the blade root suggests a difference in the way the lag damper is modelled between HOST and RCAS. The fourth harmonic of the chord bending moment remains ellusive to both calculations, whereas the third and fifth are better captured by Helios/RCAS. Overall, compared to chord bending moment, the harmonics of flap bending moment and torsion moment exhibit better agreement between calculations and with measurement.

The challenges in capturing chord bending moment were not observed in (Refs. 2, 3), where calculations were compared to the 7A rotor wind tunnel experiment. This may be related to the fact that rotor-drivetrain coupling may be smaller in the 7A rotor wind tunnel rig than in the UH-60A flight testing. It should be noted that the effects of drivetrain dynamics on the chord bending moment for the flight test and the effects of hub impedance using test stand NASTRAN model on the chord bending moment for the wind-tunnel test are also investigated for the UH-60A rotor. In general, the effects of drivetrain dynamics slightly improved both 4/rev and 5/rev harmonic magnitude correlation and the effects of hub impedance improved the correlation of both 3/rev and 4/rev harmonic components. Readers who are interested in those details are referred to (Ref. 11).

CONCLUSIONS

This work is an achievement of the cooperation between the U.S. Army and ONERA under the U.S./France Project Agreement on Rotary-Wing Aeromechanics and Human Factors Integration Research, a more than 50 year old cooperation between the United States of America and France in the field of rotorcraft.

Results support previous evidence that accounting for pitch link flexibility is an enabling factor for high-fidelity predictions of rotor loads.

The good agreement between the predictions of the two partners paves the way towards joint investigations of more challenging flight conditions and blade shapes, in order to ultimately improve the performance and loads prediction capability of high-performance, high-speed rotors.

ACKNOWLEDGMENTS

The authors would like to acknowledge the U.S./France Project Agreement on Rotary-Wing Aeromechanics and Human Factors Integration Research, a longstanding cooperation between the U.S. Army, ONERA and DGA.

REFERENCES

1. Bousman, W. G., and Kufeld, R. M., "UH-60A Airloads Catalog," Technical Report NASA/TM-2005-212827, August 2005.

2. Ortun, B., Potsdam, M., Yeo, H., and Truong, K. V., "Rotor Loads Prediction on the ONERA 7A Rotor Using Loose Fluid/Structure Coupling," *Journal of the American Helicopter Society*, Vol. 62, (3), July 2017, pp. 1–13. DOI: 10.4050/JAHS.62.032005

3. Yeo, H., Potsdam, M., Ortun, B., and Truong, K. V., "High-Fidelity Structural Loads Analysis of the ONERA 7A Rotor," *Journal of Aircraft*, Vol. 54, (5), September 2017, pp. 1825–1839. DOI: 10.2514/1.C034286

4. Yeo, H., and Potsdam, M., "Rotor Structural Loads Analysis Using Coupled Computational Fluid Dynamics/Computational Structural Dynamics," *Journal of Aircraft*, Vol. 53, (1), January 2016, pp. 87–105. DOI: 10.2514/1.C033194

5. Potsdam, M., Yeo, H., and Johnson, W., "Rotor Airloads Prediction Using Loose Aerodynamic/Structural Coupling," *Journal of Aircraft*, Vol. 43, (3), May 2006, pp. 732–742. DOI: 10.2514/1.14006

6. Saberi, H. A., Hasbun, M., Hong, J., Yeo, H., and Ormiston, R. A., "RCAS Overview of Capabilities, Validations, and Applications to Rotorcraft Problems," Proceedings of the 71st Annual Forum of the American Helicopter Society, 2015.

7. Wissink, A. M., Sitaraman, J., Jayaraman, B., Roget, B., Lakshminarayan, V. K., Potsdam, M. A., Jain, R., Bauer, A., and Strawn, R., "Recent advancements in the Helios Rotorcraft Simulation Code," *54th AIAA Aerospace Sciences Meeting*, 2016. DOI: 10.2514/6.2016-0563

8. Benoit, B., Dequin, A.-M., and Kampa, K., "HOST, a General Helicopter Simulation Tool for Germany and France," Proceedings of the 56th Annual Forum of the American Helicopter Society, 2000.

9. Cambier, L., Heib, S., and Plot, S., "The Onera elsA CFD software: input from research and feedback from industry," *Mechanics & Industry*, Vol. 14, (3), 2013, pp. 159–174. DOI: 10.1051/meca/2013056

10. Biedron, R. T., and Lee-Rausch, E. M., "An Examination of Unsteady Airloads on a UH-60A Rotor: Computation versus Measurement," Proceedings of the 68th Annual Forum of the American Helicopter Society, 2012.

11. Yeo, H., "UH-60A Rotor Structural Loads Analysis with Fixed-System Structural Dynamics Modeling," *Journal of Aircraft*, Vol. 56, (2), March 2019, pp. 669–684. DOI: 10.2514/1.C035102

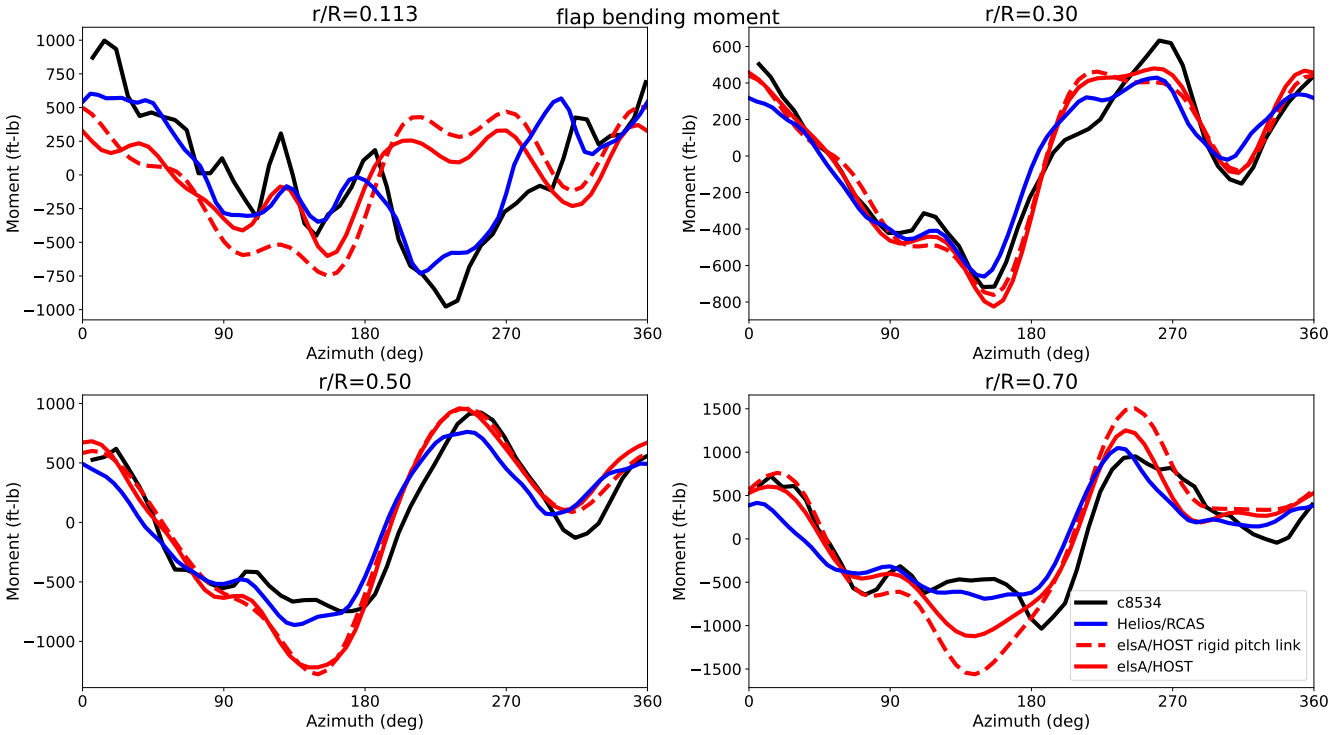

Figure 9. c8534. Comparison of flap bending moment. Means removed.

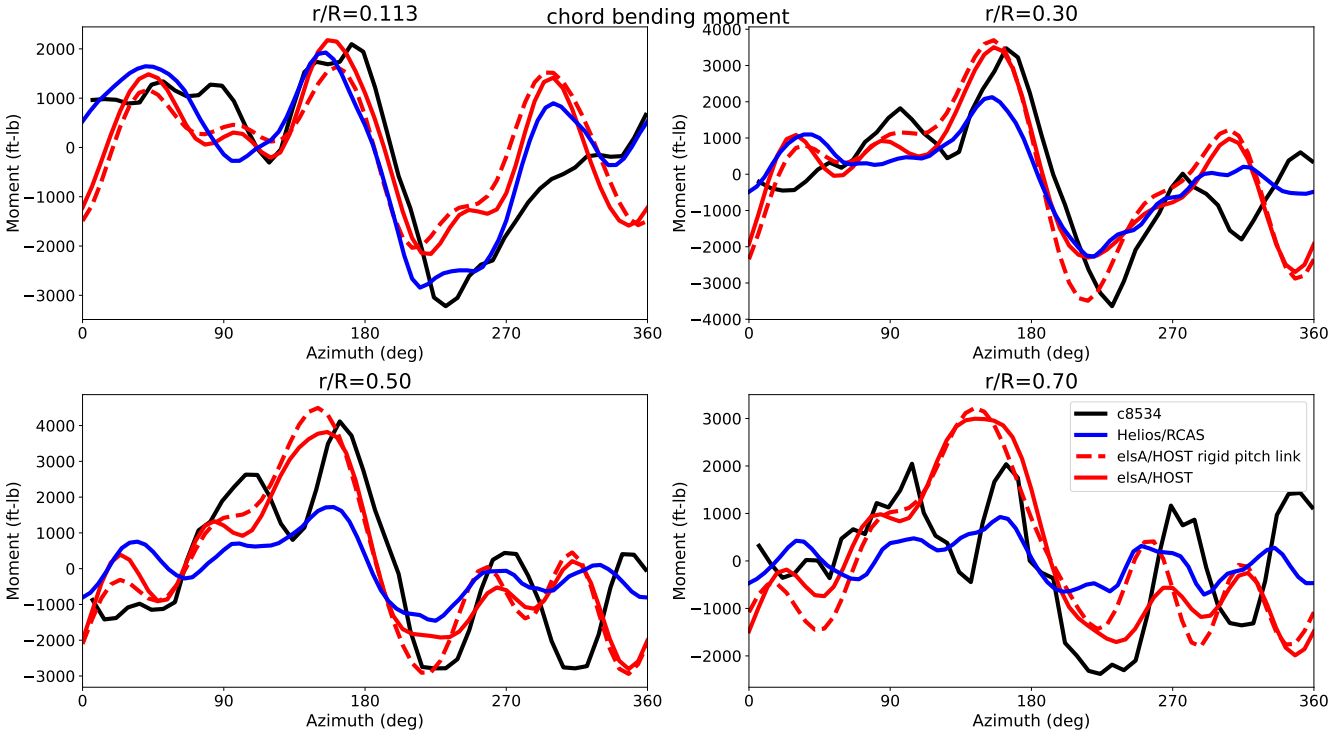

Figure 10. c8534. Comparison of chord bending moment. Means removed.

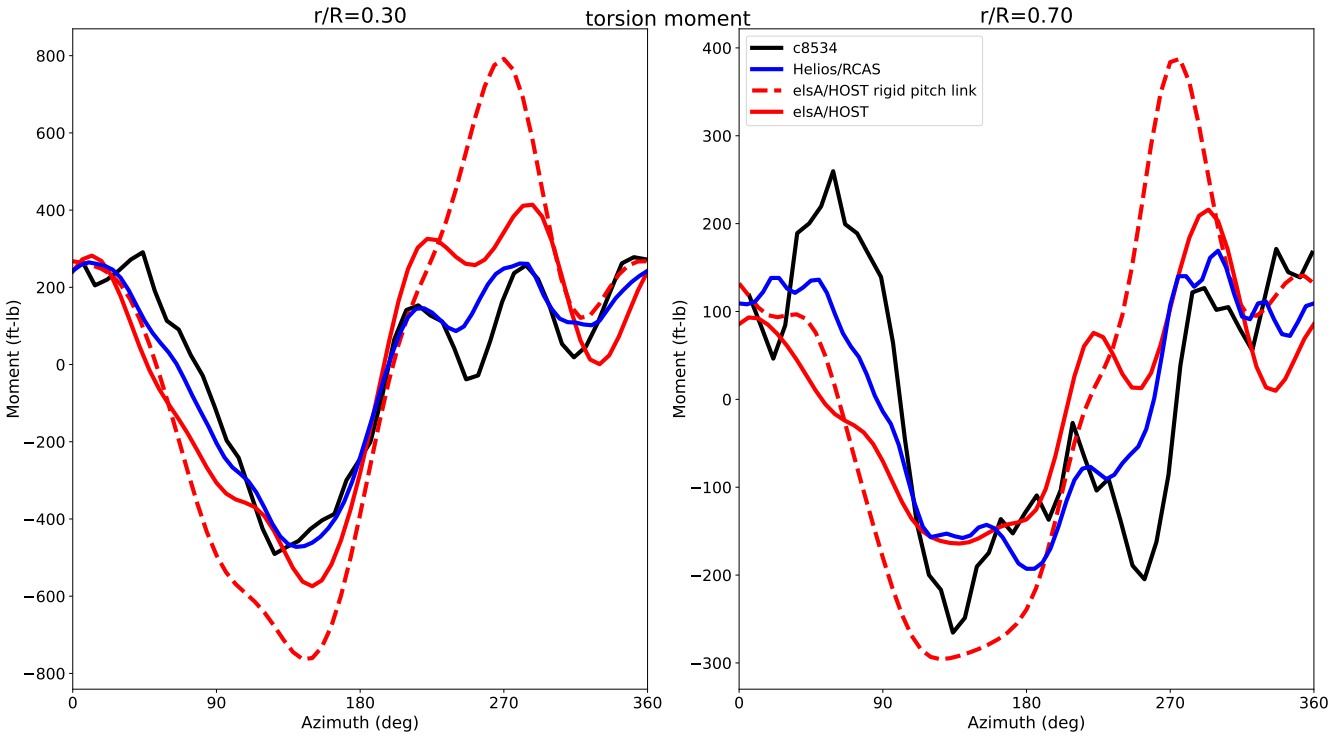

Figure 11. c8534. Comparison of torsion moment. Means removed.

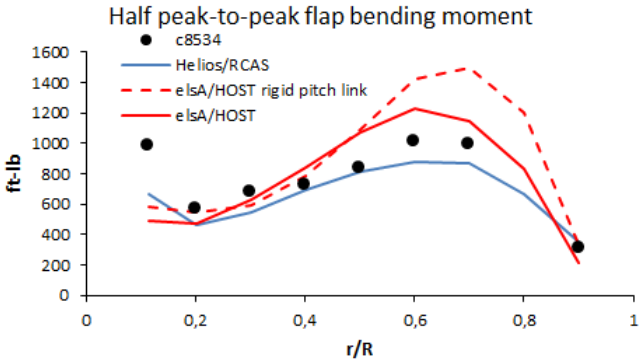

Figure 12. c8534. Flap bending moment.

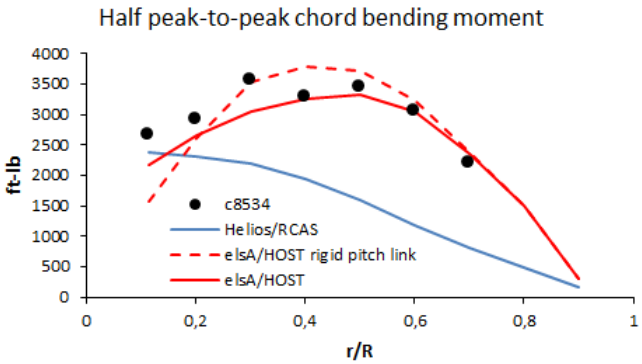

Figure 13. c8534. Chord bending moment.

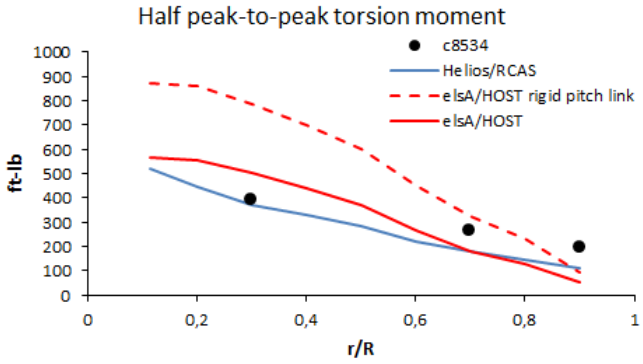

Figure 14. c8534. Torsion moment.

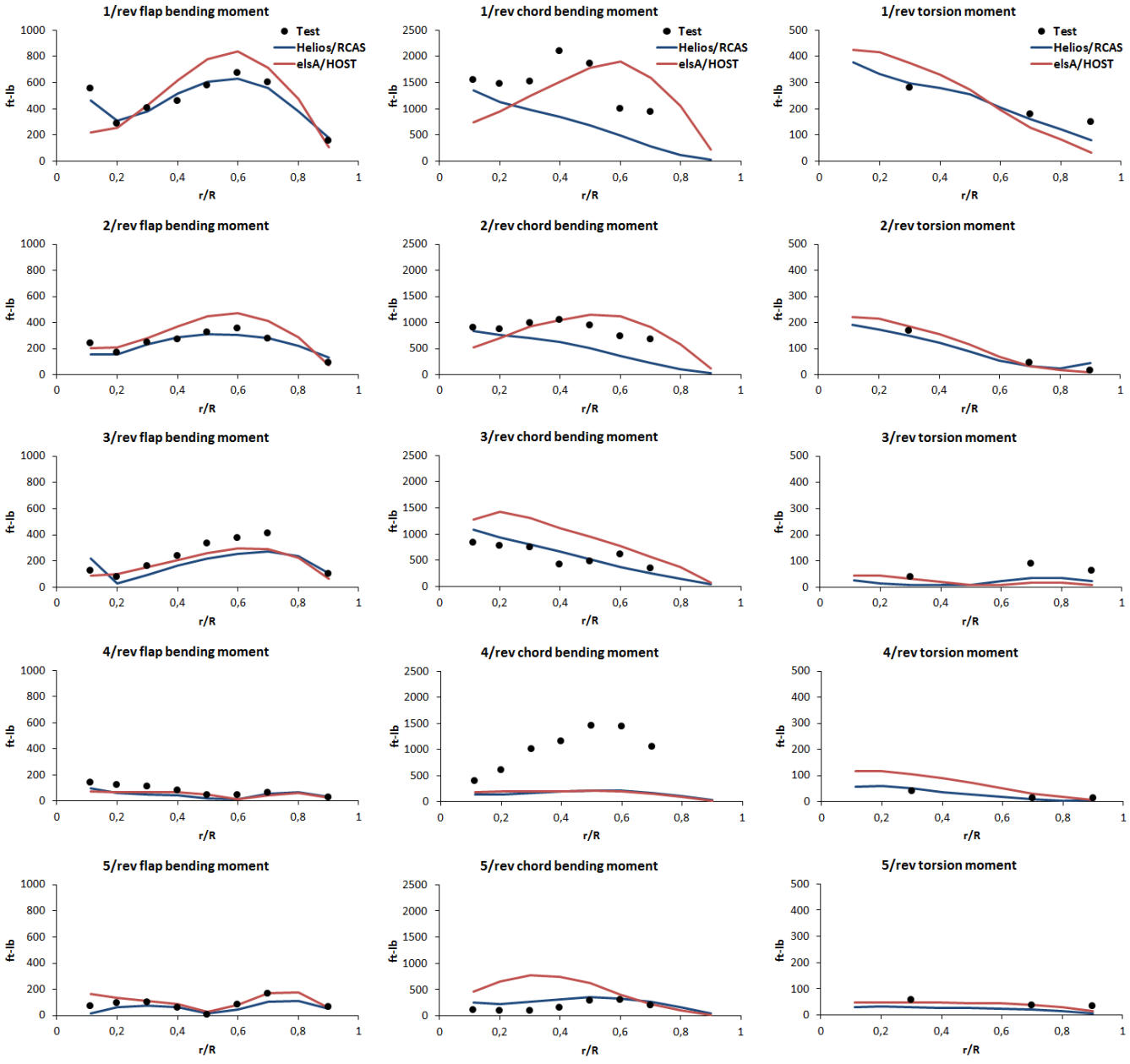

Figure 15. c8534. Comparison of harmonic magnitude of calculated and measured structural loads.